Published in final edited form as:

J Am Chem Soc. 2018 March 28; 140(12): 4191–4194. doi:10.1021/jacs.7b12707.

Observation of Radical Rebound in a Mononuclear Nonheme Iron Model Complex

Thomas M. Pangia[†], **Casey G. Davies**[‡], **Joshua R. Prendergast**[‡,∫], **Jesse B. Gordon**[†], **Maxime A. Siegler**[†], **Guy N. L. Jameson**[*,‡,∫], and **David P. Goldberg**[*,†]

[†]Department of Chemistry, The Johns Hopkins University, Baltimore Maryland, 21218

[‡]Department of Chemistry and MacDiarmid Institute for Advanced Materials and Nanotechnology, University of Otago, P.O. Box 56, Dunedin 9054, New Zealand [∫]School of Chemistry, Bio21 Molecular Science and Biotechnology Institute, The University of Melbourne, 30 Flemington Road, Parkville, Victoria 3010, Australia

Abstract

A nonheme iron(III) terminal methoxide complex, $[Fe^{III}(N3PyO^{2Ph})(OCH_3)]ClO_4$, was synthesized. Reaction of this complex with the triphenylmethyl radical (Ph_3C•) leads to formation of Ph_3COCH_3 and the one-electron reduced iron(II) center, as seen by UV-vis, EPR, ^{1}H NMR, and Mössbauer spectroscopy. These results indicate that homolytic Fe-O bond cleavage occurs together with C-O bond formation, providing a direct observation of the “radical rebound” process proposed for both biological and synthetic nonheme iron centers.

Reserve for TOC

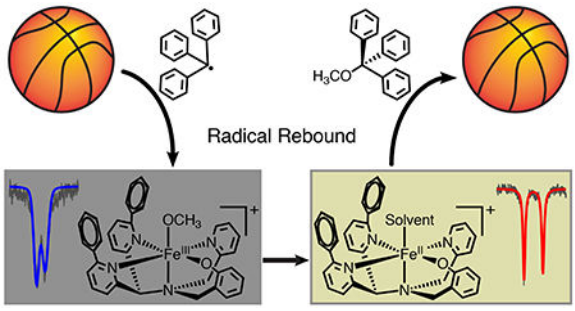

The radical rebound mechanism is a useful paradigm to explain C-H hydroxylations carried out by both heme and nonheme oxygenases, as well as analogous synthetic complexes.[1] The mechanism involves the abstraction of a hydrogen atom from a C-H bond by a high-valent metal-oxo species, followed by recombination of the carbon radical (R•) with the newly

[*]Corresponding Authors: dpg@jhu.edu; guy.jameson@unimelb.edu.au.

ASSOCIATED CONTENT

Supporting Information. Syntheses, spectroscopy, X-ray crystallographic files (CIF) are available free of charge via the Internet at http://pubs.acs.org.

The authors declare no competing financial interest.

formed metal-bound hydroxide ligand. The recombination, or “rebound” step, is presumed to involve homolytic cleavage of the Fe-O bond along with one-electron reduction of the iron center and formation of the new C-O bond (Scheme 1). The C-H cleavage step is typically rate-determining, making the rebound step too fast for direct observation. Efforts to probe this step indirectly have come from a number of experimental and computational studies.[2] Alternative pathways to OH rebound are also possible, including radical dissociation in the synthetic systems and trapping by other reactive species (e.g. O_2). [2a]

The rebound step is especially important for the nonheme iron halogenases (e.g. SyrB2, CytC3, WelO5).[3] These enzymes selectively transfer a halogen ligand over an OH ligand in the putative rebound step, and the question of how these enzymes direct halogenation, versus the more common hydroxylation seen for the hydroxylases, has been the focus of synthetic model studies.[4]

Synthetic nonheme model systems involving high-valent Fe(O) species have provided evidence for both rebound and non-rebound pathways in C-H oxidations.[5] Related computational studies have shown that when radical dissociation rates are competitive with rebound rates, a nonrebound mechanism may prevail, and possible causes for this reactivity were suggested.[2a]

The factors that control the rebound process, and sometimes result in nonrebound pathways, are critical in determining the final outcome of nonheme iron-mediated oxidations. For example, substrate orientation has been invoked as a key factor influencing rebound in the nonheme iron halogenases.[3] However, first-coordination sphere effects, such as the identity of the coligands on Fe, the relative metal-O(X) bond strengths, Fe redox potentials, and the electronic structure of the Fe complex all may have a significant influence over directing rebound versus non-rebound reactivity in both enzymes and synthetic catalysts.

We have initiated efforts to develop complexes in which the rebound step can be directly interrogated. We recently described the first example of such a system for a heme-related iron-hydroxide complex.[6] However, to our knowledge there has thus far been no direct observation of a radical rebound reaction with nonheme iron to produce a new C-O bond.[7] Herein we report the synthesis and structural characterization of a rare, terminal iron(III)-methoxide complex, and show that it reacts directly with stabilized carbon radicals to give a methoxy ether and a reduced iron(II) complex.

Previous work from our lab described a pentadentate ligand, N3PyS, that produced a mononuclear iron(II) complex which reacted readily with O_2 and NO.[8] It was shown that incorporation of the single thiolato donor facilitated O_2 reactivity.[9] Reaction of $[Fe^{II}(N3PyS)](BF_4)$ with O_2 led to S-oxygenation.[8]

For the current study, we replaced the phenylthiolate arm with a phenoxo donor and added phenyl substituents to give the new ligand $N3PyOH^{2Ph}$ (Scheme 2), with the objective of maintaining the electron-rich nature of the Fe^{II} center for O_2 reactivity while avoiding ligand oxygenation. The bulky phenyl groups were incorporated to discourage μ-oxo dimer formation. The unsubstituted analog N3PyOH gives an oxo-bridged diferric complex from

Fe^{II} and O_2.[10] A similar diphenyl-substituted N4Py system has led to our recent isolation and structural characterization of a metastable $Fe^{IV}(O)$ complex.[11]

Reaction of $N3PyOH^{2Ph}$ with $Fe^{II}(ClO_4)_2$ and base in acetonitrile led to the isolation of a high-spin mononuclear Fe^{II} complex, $[Fe^{II}(N3PyO^{2Ph})(CH_3CN)](ClO_4)$ (**1**) (Scheme 2). Dark yellow crystals were grown from $MeOH/Et_2O$, resulting in the crystal structure shown in Figure 1. The ligand binds pentadentate to Fe^{II}, while the sixth site is occupied by acetonitrile. The Fe-N distances in **1** are similar to the Fe-N distances found in high-spin Fe^{II} complexes of both N3PyS and $N4Py^{2Ph}$ derivatives, with the exception of the phenyl-substituted pyridine donor trans to the phenolate group, which exhibits an elongated distance of 2.473(3) Å. A similarly elongated distance is seen for one of the phenyl-pyridyl donors (Fe-N = 2.378(13) Å) in $[Fe^{II}(N4Py^{2Ph})(NCCH_3)](BF_4)_2$.[11a] The Fe-O distance in **1** is in line with other Fe^{II}-OAr complexes.[12]

Reaction of **1** with air in methanol leads to a slow color change from dark yellow **1** to a new dark purple species. UV-vis spectroscopy shows the conversion of **1** to a new spectrum with a broad band at 550 nm (ε = 1290 M^{-1} cm^{-1}), which is consistent with a phenolate-to-iron(III) charge-transfer transition.[13] Crystallization of the purple product from $MeOH/Et_2O$ led to the crystal structure shown in Figure 1. The structure reveals an iron(III) complex with a terminal methoxide ligand in the open site, with formula $[Fe^{III}(N3PyO^{2Ph})(OCH_3)](ClO_4)$ **(2**) (Scheme 2). Crystals of **2** were examined by EPR spectroscopy, and revealed a relatively sharp feature at g = 4.26 (13 K, THF). This spectrum is consistent with a high-spin Fe^{III} (S = 5/2) ground state. An Evans method measurement[14] of **2** in THF-d_8 gave μ_{eff} = 5.3 μ_B, close to the spin-only value (5.91 μ_B) for a mononuclear high-spin Fe^{III} ion. The distance of the Fe-N bond for the phenyl-substituted pyridine donor trans to the phenolate donor of **2** is shorter than the same bond in **1** (2.341(2) Å vs. 2.473(3) Å), as expected for the increase in oxidation state. Terminal iron-alkoxide complexes are relatively rare. The closest analog to **2** is $Fe^{III}(N4Py)(OCH_3)]^{2+}$.[15] The Fe-$OCH_3$ bond length for **2** of 1.784(2) Å) is similar when compared to the same bond in the closest analog, $Fe^{III}(N4Py)(OCH_3)]^{2+}$ (1.772(3) Å), and is on the short end of the range seen for other Fe^{III}-OCH_3 complexes (Fe^{III}-O: 1.77–1.90 Å).[15–16]

Given that **2** is a close analog of the $Fe^{III}(OH)$ rebound intermediate in Scheme 1, we hypothesized that **2** could be used for the direct examination of a radical rebound process. A suitable carbon radical (R•) might react with **2** to give a methoxy ether ($ROCH_3$) product and the one-electron reduced iron(II) complex. Trityl radical (Ph_3C•) is stable in organic solvents, and readily prepared in the solid state as a closed-shell dimer $(Ph_3C)_2$ (Gomberg's dimer), which dissociates to give a known amount of the radical (~2% at 25 °C) in solution.[17] Reaction of $(Ph_3C)_2$ with **2** in THF at 23 °C led to the slow decay (~48 h) of the Fe^{III}-OCH_3 complex as seen by UV-vis spectroscopy. At higher temperatures, Gomberg's dimer dissociates to a greater extent,[17] and heating the former reaction to 50 °C led to ~80% decay of the 570 nm band for **2** within 1 h (Figure S7). Monitoring the same reaction by EPR spectroscopy showed that the singlet at g = 4.26 assigned to **2** decreases upon reaction with Ph_3C•, with an 80% loss of **2** after 1 h at 50 °C (Figure S9), in good agreement with the UV-vis data. The final product is EPR-silent, consistent with integer-spin Fe^{II}, the anticipated product.

Thin-layer chromatography (TLC) indicated that the rebound product Ph_3COCH_3 was formed after 1 h in reaction mixtures of **2** and $(Ph_3C)_2$ in THF at 50 °C. Analysis by ^1H NMR spectroscopy in THF-d_8 revealed the formation of a peak at δ 3.04 ppm after 60 min (Figure S13) which can be assigned to Ph_3COCH_3. Quantitation of this peak gave a yield of the methoxy ether of 60% (based on total **2**). This result was corroborated by GC-FID, which revealed production of Ph_3COCH_3 in 58% yield. The GC and NMR yields are in good agreement with each other. Further improvements in yield could not be obtained by increasing reaction times up to 24 h. The yield for this reaction is likely limited by the concomitant formation of a side product of the trityl radical, which was identified by ^1H NMR as a tautomeric form of Gomberg's dimer that does not dissociate to release trityl radical,[18] as well as slow background decomposition of **2** under the reaction conditions (Figure S8).

Mössbauer spectroscopy provided further insights regarding the rebound reaction of **2** with trityl radical. Isotope-enriched **2** (^{57}Fe, 95.93%) was reacted with Gomberg's dimer in THF at 50 °C for 70 min, and then frozen at 77 K for Mössbauer analysis (Figure 2). The spectrum of **2** before reaction, measured at 5.2 K, shows a 6-line pattern typical of a magnetically split iron(III) complex, overlaid with a quadrupole doublet. These signals are consistent with a mixture of Fe^{III} in both slow- and fast-relaxation regimes, respectively. This analysis was confirmed when the sample was measured at 100 K (Figure 2), showing that the sextet collapsed into a single quadrupole doublet with parameters consistent with high-spin Fe^{III} ($\delta = 0.50$, $\Delta E_Q = 1.29$ mm s^{-1}). The Mössbauer spectrum of a solid state sample of **2** at 100 K is nearly identical (Figure S17), further corroborating this analysis. Upon reaction with $Ph_3C•$, the Fe^{III} starting material disappears, and a new, sharp quadrupole doublet with parameters $\delta = 1.38$ and $\Delta E_Q = 3.35$ mm s^{-1} is observed. The parameters of this new doublet are distinctive of high-spin iron(II), and quantification of the signal indicates that the final Fe^{II} species accounts for 90% of the total iron content. This result indicates that the slow background decay of **2** gives the same one-electron reduced Fe^{II} product.

A Mössbauer spectrum of a recrystallized sample of **1** in THF shows a high-spin Fe^{II} quadrupole doublet ($\delta = 1.05$, $\Delta E_Q = 2.29$ mm s^{-1}), albeit with different parameters than the final reaction mixture described above. The differences observed between this spectrum and the final reaction mixture are most likely due to different solvent ligands occupying the sixth site of $[Fe^{II}(N3PyO^{2Ph})]^+$. A THF solvent molecule likely occupies the open site in the reaction with $Ph_3C•$, as compared to the coordinated CH_3CN seen in **1**. To gain further insight, DFT calculations were performed on optimized geometries of **1**, **1-THF**, and a 5-coordinate analog of **1**. The calculated isomer shift of a 5-coordinate complex is lower than both the experimental data and calculated 6-coordinate complexes (Table S3). DFT calculations also show the isomer shift of **1-THF** is higher than that for **1**, as seen experimentally. Thus, DFT calculations support that a 6-coordinate product is formed. This analysis is further supported by paramagnetic ^1H NMR, which revealed that the initial spectrum for **2**, with peaks between +100 and –40 ppm, disappears upon reaction with trityl radical, leaving poorly-resolved features. However, removal of the THF and dissolution of

the remaining brown residue in CD_3CN gives an NMR spectrum that can be assigned to the acetonitrile-bound Fe^{II} complex (Figure S14).

Taken together, the UV-vis, EPR, NMR and Mössbauer data confirm that **2** reacts with Ph_3C• to give the one-electron-reduced, radical rebound product $[Fe^{II}(N3PyO^{2Ph})]^+$ and a new C-O bond. The rebound reaction is summarized in Scheme 3. In our work on Fe(OH) rebound with trityl radical, we have shown that a concerted rebound mechanism is the most likely scenario.[6] We suggest a similar mechanism here, as shown in Scheme 3.

The synthesis and structural characterization of a rare, mononuclear terminal Fe^{III}-methoxide complex allowed for the first direct observation of radical rebound with a nonheme iron complex to give a new C-O bond. The Fe^{III}-OCH_3 complex reacts efficiently with trityl radical in a rebound process that involves homolytic cleavage of the Fe-O bond and formation of Ph_3COCH_3 and the one-electron-reduced iron(II) complex. The current work provides support for the feasibility of the rebound pathway in C-H activation processes by nonheme iron-oxo species. However the probability of rebound versus cage escape of the carbon radical is a key question that remains challenging to assess. The direct examination of the radical rebound reaction described here foreshadows further experimental approaches to address these fundamental mechanistic issues.

Supplementary Material

Refer to Web version on PubMed Central for supplementary material.

ACKNOWLEDGMENT

The NIH (GM119374 to D.P.G. and G.N.L.J.) is gratefully acknowledged for financial support. G.N.L.J. further thanks the University of Otago and the Faculty of Science, the University of Melbourne for financial support.

REFERENCES

(1). (a) Huang X, Groves JT. J. Biol. Inorg. Chem. 2017; 22:185–207. [PubMed: 27909920] (b) Ortiz de Montellano PR. Chem. Rev. 2010; 110:932–948. [PubMed: 19769330] (c) Kovaleva EG, Lipscomb JD. Nat. Chem. Biol. 2008; 4:186–193. [PubMed: 18277980]

(2). (a) Cho KB, Hirao H, Shaik S, Nam W. Chem. Soc. Rev. 2016; 45:1197–210. [PubMed: 26690848] (b) Shaik S, Kumar D, de Visser SP, Altun A, Thiel W. Chem. Rev. 2005; 105:2279–2328. [PubMed: 15941215]

(3). (a) Mitchell AJ, Zhu Q, Maggiolo AO, Anath NR, Hillwig ML, Liu X, Boal AK. Nat. Chem. Biol. 2016; 12:636–640. [PubMed: 27348090] (b) Matthews ML, Neumann CS, Miles LA, Grove TL, Booker SJ, Krebs C, Walsh CT, Bollinger JM Jr.. Proc. Natl. Acad. Sci. 2009; 106:17723–17728. [PubMed: 19815524] (c) Martinie RJ, Livada J, Chang W.-c., Green MT, Krebs C, Bollinger JM Jr., Silakov A. J. Am. Chem. Soc. 2015; 137:6912–6919. [PubMed: 25965587] (d) Wong C, Fujimori DG, Walsh CT, Drennan CL. J. Am. Chem. Soc. 2009; 131:4872–4879. [PubMed: 19281171]

(4). (a) Planas O, Clemancey M, Latour J-M, Company A, Costas M. Chem. Commun. 2014; 50:10887–10890.(b) Puri M, Biswas AN, Fan R, Guo Y, Que L Jr.. J. Am. Chem. Soc. 2016; 138:2484–2487. [PubMed: 26875530]

(5). (a) Cho K-B, Wu X, Lee Y-M, Kwon YH, Shaik S, Nam W. J. Am. Chem. Soc. 2012; 134:20222–20225. [PubMed: 23205855] (b) Bae SH, Seo MS, Lee YM, Cho KB, Kim WS, Nam W. Angew. Chem. Int. Ed. Engl. 2016; 55:8027–8031. [PubMed: 27273456] (c) Rana S, Dey A, Maiti D. Chem. Commun. 2015; 51:14469–14472.

(6). Zaragoza JPT, Yosca TH, Siegler MA, Moënne-Loccoz P, Green MT, Goldberg DP. J. Am. Chem. Soc. 2017; 139:13640–13643. [PubMed: 28930448]

(7). (a) Kojima T, Nakayama K, Ikemura K, Ogura T, Fukuzumi S. The observation of metal-bound C-O products following a related rebound process for a nonheme $Ru^{IV}(O)$ complex was described J. Am. Chem. Soc. 2011; 133:11692–11700. [PubMed: 21696162] (b) Smith JM, Mayberry DE, Margarit CG, Sutter J, Wang H, Meyer K, Bontchev RP. J. Am. Chem. Soc. 2012; 134:6516–6519. [PubMed: 22452612] (c) Jang ES, McMullin CL, Kass M, Meyer K, Cundari TR, Warren TH. J. Am. Chem. Soc. 2014; 136:10930–10940. [PubMed: 24940616] (d) Iovan DA, Betley TA. J. Am. Chem. Soc. 2016; 138:1983–1993. [PubMed: 26788747]

(8). McQuilken AC, Jiang Y, Siegler MA, Goldberg DP. J. Am. Chem. Soc. 2012; 134:8759–8761.

(9). Draksharapu A, Li Q, Roelfes G, Browne WR. Dalton Trans. 2012; 41:13180–13190. [PubMed: 23011515]

(10). (a) Ligtenbarg AGJ, Oosting P, Roelfes G, La Crois RM, Lutz M, Hage R, Spek AL, Feringa BL. Chem. Commun. 2001:385–386.(b) Unjaroen D, Swart M, Browne WR. Inorg. Chem. 2017; 56:470–479. [PubMed: 27935682]

(11). (a) Sahu S, Widger LR, Quesne MG, de Visser SP, Matsumura H, Moënne-Loccoz P, Siegler MA, Goldberg DP. J. Am. Chem. Soc. 2013; 135:10590–10593. [PubMed: 23834409] (b) Sahu S, Zhang B, Pollock CJ, Durr M, Davies CG, Confer AM, Ivanović-Burmazović I, Siegler MA, Jameson GNL, Krebs C, Goldberg DP. J. Am. Chem. Soc. 2016; 138:12791–12802. [PubMed: 27656776]

(12). Boyle TJ, Ottley LAM, Apblett CA, Stewart CA, Hoppe SM, Hawthorne KL, Rodriguez MA. Inorg. Chem. 2011; 50:6174–6182. [PubMed: 21635011]

(13). Shakya R, Allard MM, Johann M, Heeg MJ, Rentschler E, Shearer JM, McGarvey B, Verani CN. Inorg. Chem. 2011; 50:8356–8366. [PubMed: 21805957]

(14). (a) Evans DF, Jakubovik DA. J. Chem. Soc. Dalton Trans. 1988:2927–2933.(b) Confer AM, Mcquilken AC, Matsumura H, Möenne-Loccoz P, Goldberg DP. J. Am. Chem. Soc. 2017; 139:10621–10624. [PubMed: 28749673]

(15). Roelfes G, Lubben M, Chen K, Ho RYN, Meetsma A, Genseberger S, Hermant RM, Hage R, Mandal SK, Young VG Jr., Zang Y, Kooijman H, Spek AL, Que L Jr., Feringa BL. Inorg. Chem. 1999; 38:1929–1936. [PubMed: 11670967]

(16). (a) Jonas RT, Stack TDP. J. Am. Chem. Soc. 1997; 119:8566–8567.(b) Chang K-C, Huang C-J, Chang Y-H, Wu Z-H, Kuo T-S, Hsu H-F. Inorg. Chem. 2016; 55:566–572. [PubMed: 26699874] (c) Moon D, Lah MS. Inorg. Chem. 2002; 41:4708–4714. [PubMed: 12206694] (d) Kerber WD, Perez KA, Ren C, Siegler MA. Inorg. Chem. 2014; 53:11507–11516. [PubMed: 25322447]

(17). (a) Gomberg M. J. Am. Chem. Soc. 1914; 36:1144–1170.(b) Ihde AJ. Pure Appl. Chem. 1967; 15:1–14.

(18). Chen C, Lee H, Jordan RF. Organometallics. 2010; 29:5373–5381.

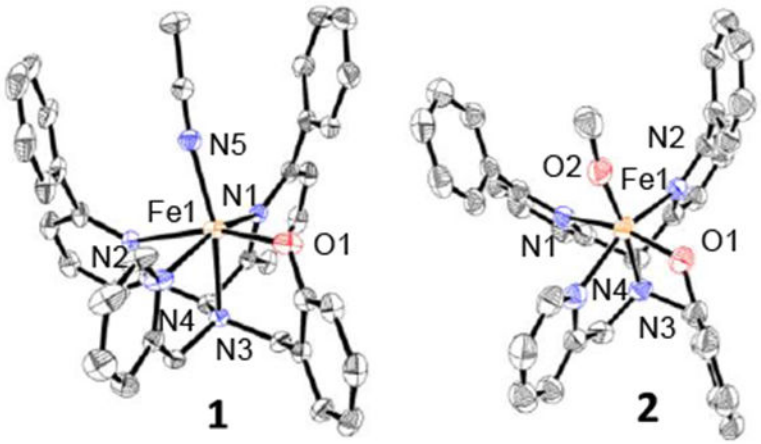

Figure 1.

Displacement ellipsoid plots (50% probability) of the cations of **1** and **2** at 110(2) K. H atoms are not shown for clarity.

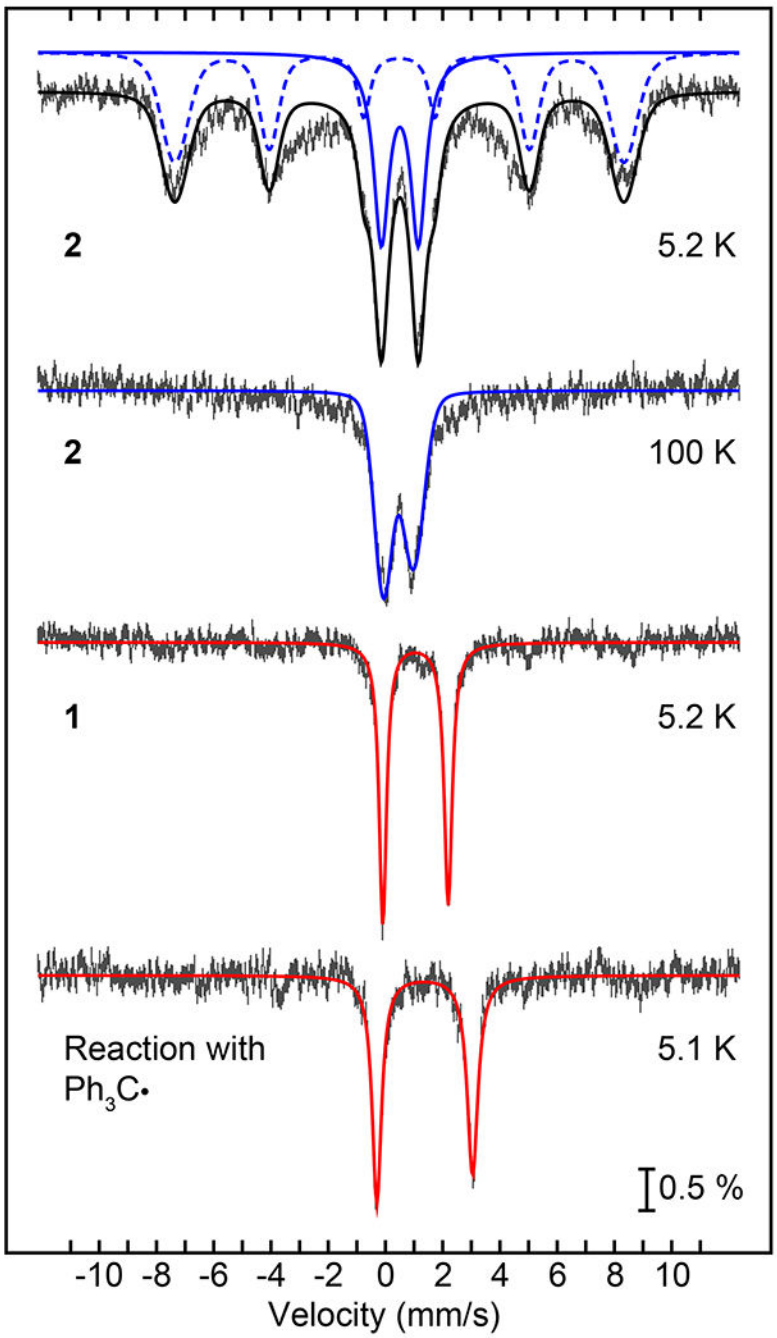

Figure 2.

^{57}Fe Mössbauer spectra (hatched lines) for: complex **2** in THF at 5.2 K together with the best fits for hs-Fe^{III} in both the slow-(blue dashed line) and fast-relaxing (blue solid line) regimes (top); same sample as in (top) at 100 K and best fit (blue line) for a fast-relaxing quadrupole doublet as the major component (top middle); complex **1** in THF at 5.2 K and best fit (red line) for a hs-Fe^{II} quadrupole doublet (bottom middle); the reaction mixture of **2** and Gomberg's dimer in THF at 50 °C after 70 min and best fit (red line) for a hs-Fe^{II} quadrupole doublet (bottom).

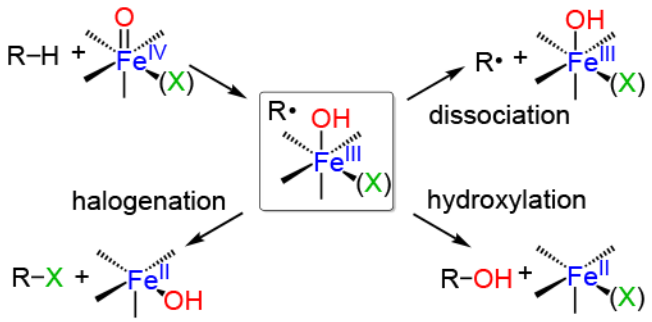

Scheme 1. Oxygen and Halogen Radical Rebound Mechanisms

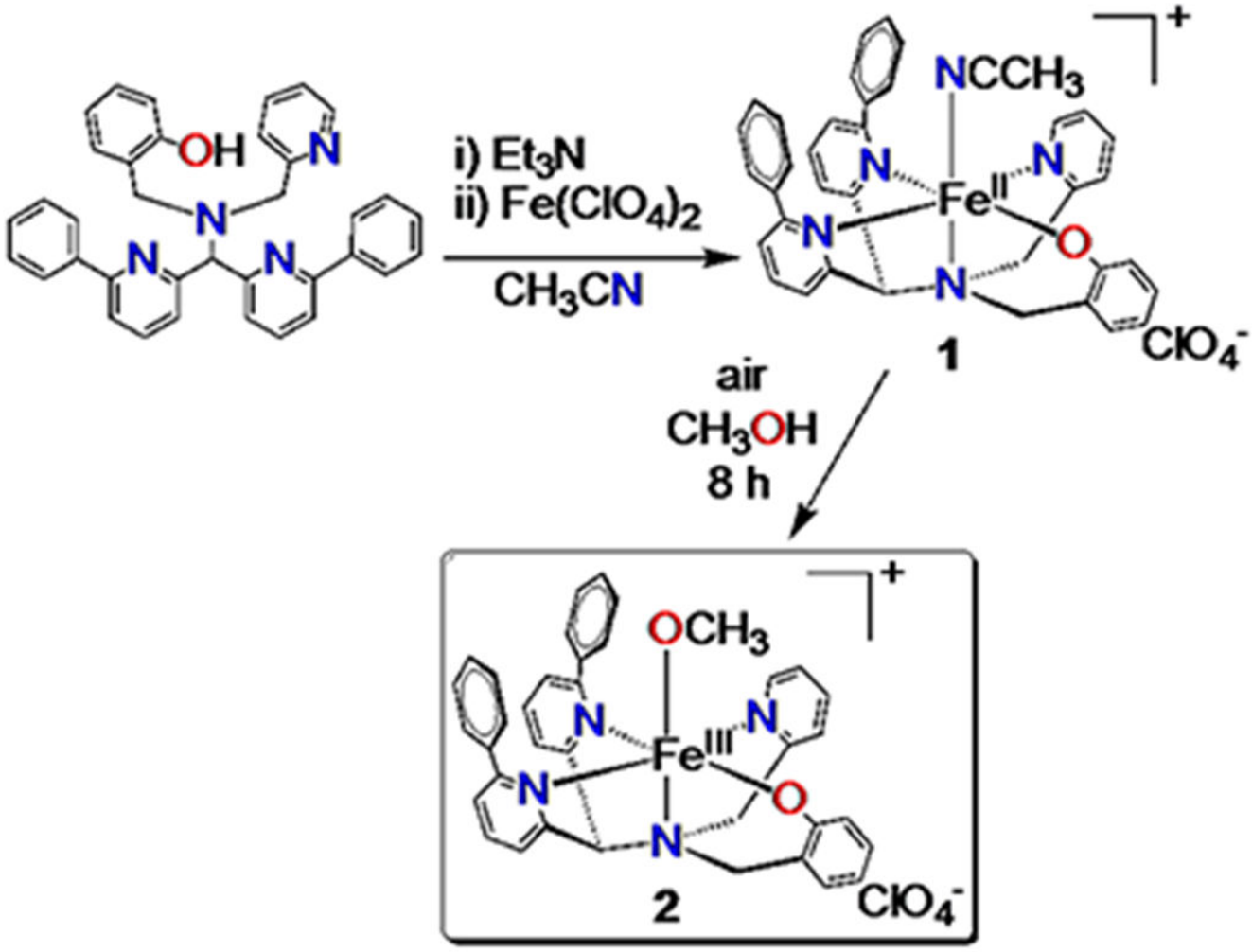

Scheme 2. Synthesis of $[Fe^{II}(N_3PyO^{2Ph})(CH_3CN)](ClO_4)$ (1) and $[Fe^{III}(N_3PyO^{2Ph})(OCH_3)](ClO_4)$ (2)

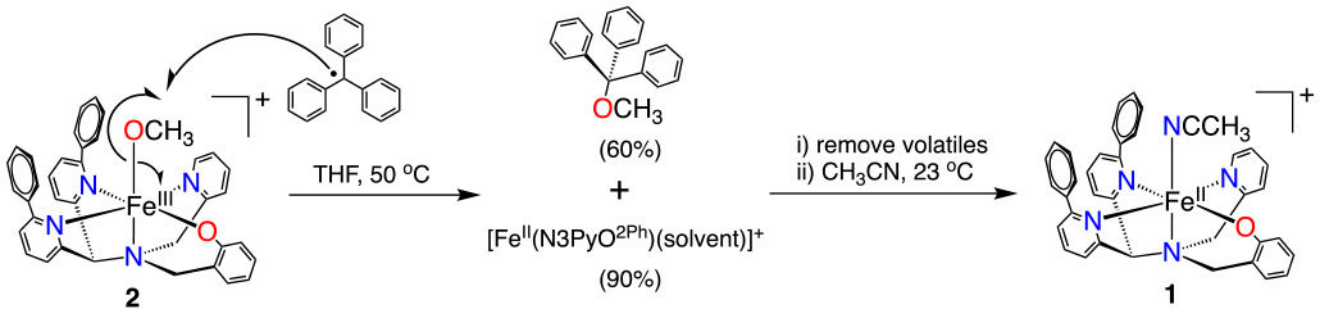

Scheme 3. Radical Rebound Reaction